Investigation of the paramagnetic centres and electronic properties of silicon carbide nanomaterials

1999 J. Phys.: Condens. Matter 11 4887

(http://iopscience.iop.org/0953-8984/11/25/308)

J. Phys.: Condens. Matter **11** (1999) 4887–4897. Printed in the UK PII: S0953-8984(99)97721-4

Investigation of the paramagnetic centres and electronic properties of silicon carbide nanomaterials

S Charpentier†, A Kassiba†, J Emery† and M Cauchetier‡

† Laboratoire de physique de l'état condensé UPRESA-6087, Université du Maine, Faculté des sciences, Avenue Olivier Messiaen, 72017 Le Mans Cedex, France

‡ CEA-DRECAM, Service des Photons, Atomes et Molecules, CE Saclay, Gif sur Yvette, France

Received 21 September 1998, in final form 22 April 1999

Abstract. Ultrafine powders of silicon carbide (SiC) exhibit a substantial electric conductivity ($\sigma_{dc} \sim 0.05$ S cm^{-1}) after annealing at temperatures between 1500 °C and 1800 °C. The origin of this phenomena is discussed with respect to structural modifications, sample composition and the delocalized paramagnetic centres involved in these materials. The structural evolution of SiC nanomaterials with annealing was monitored by ^{29}Si and ^{13}C Magic Angle Spinning Nuclear Magnetic Resonance (MAS NMR). A consistent analysis of the electron paramagnetic resonance (EPR) spectra was performed and showed the coexistence of two paramagnetic centres (DI, DII) localized in the crystalline sites of the SiC polytypes. Delocalized DIII paramagnetic species were partially created by thermal conversions of DII defects with energies not exceeding 13 meV. The spin susceptibility, deduced from EPR measurements, was found to be marked by delocalized paramagnetic species above 150 K and by strongly correlated (DIII) unpaired spins around 30 K. An attempt is made to correlate the delocalized unpaired spins with the electric properties of these materials.

1. Introduction

SiC-based nanocomposites show a better thermal and mechanical performance than their equivalent microcomposite counterparts [1, 2]. A second interesting feature of these materials involves the electric properties induced in such materials by annealing at high temperatures (1500 °C–1800 °C). This work is devoted to a study of the origin of these electric properties through analysis of the material structure, composition and the nature of the involved paramagnetic centres at different annealing stages.

The synthesis process by CO_2 laser pyrolysis of a gaseous mixture, initially demonstrated by Haggerty [3], was developed at the C.E.A. by Cauchetier [4, 5] to obtain SiC nanopowders from the pyrolysis of (SiH_4, C_2H_2) gaseous mixtures. Three SiC batches, differing in their fabrication conditions (residence time of the reactants in the laser beam, laser power), exhibit a common behaviour after annealing. In particular, substantial electrical conductivity ($\sigma_{dc} \sim 0.05$ S cm^{-1}) is observed when the samples are annealed above the critical temperature ($T_a = 1500$ °C) [6].

The local crystalline order is characterized by ^{29}Si and ^{13}C Magic Angle Spinning (MAS) Nuclear Magnetic Resonance (NMR). ^{29}Si and ^{13}C with a nuclear spin of $I = 1/2$ are sensitive to chemical shifts, dipolar and hyperfine interactions, and the MAS method averages out these interactions that can nevertheless be efficient for the relaxation. Thus, NMR line positions

0953-8984/99/254887+11$19.50

depend only on the isotropic chemical shift parameters. By using this method we were able to quantify the ratio of crystalline SiC polytypes, the rate of amorphous SiC and the content of carbon excess following annealing.

The electron paramagnetic resonance (EPR) technique assesses the concentration and nature of paramagnetic defects in materials. The spin susceptibility χ_s, which is proportional to the EPR spectrum integrated intensity, is determined as a function of the annealing temperature (1200 °C–1800 °C) and the sample temperature (4 K–300 K). Delocalized centres above 150 K and strongly correlated unpaired spins around 30 K characterize the χ_s features. Furthermore, by using different EPR frequency bands and a consistent numerical analysis of EPR spectra, we have shown that three paramagnetic centres (DI, DII and DIII) coexist in these SiC systems. A conversion between the paramagnetic centres localized in the SiC crystalline sites (DI, DII) and delocalized (DIII) species is thermally activated by low energies not exceeding 13 meV. We discuss here the correlation between the delocalized paramagnetic centres and the electronic properties of these nanomaterials.

2. Experimental details

SiC nanometric powders were synthesized by CO_2 laser pyrolysis of (SiH_4, C_2H_2) gaseous mixtures following [4]. Three SiC batches (SiC163, SiC177 and SiC212), differing by the residence time of the reactants in the laser beam in their preparation, were investigated. Annealing from 1200 to 1800 °C was realized in a high-temperature graphite furnace for 1 h in an argon atmosphere. Common behaviour was found at the same annealing stages and we thus limit the forthcoming discussion to the batch referred to as SiC212. Chemical analysis of the as-formed powder and after annealing, is reported in table 1. The mean particle diameter, $d_g(T)$, increases with annealing and the results in SiC212 (table 2) are marked by a jump from 54 nm to 390 nm at the critical temperature $T_a = 1500$ °C. In passing, we note that the variation of $d_g(T)$ was not so important in the SiC163 and SiC177 batches, i.e. in SiC163 $d_g(1400\,°C) = 62$ nm and $d_g(1500\,°C) = 100$ nm and in SiC177 $d_g(1400\,°C) = 150$ nm and $d_g(1500\,°C) = 196$ nm.

Table 1. Chemical analysis (wt%) of the as-formed SiC nanomaterials (SiC212) and after annealing at 1800 °C.

	Si	C	O	SiO	SiC	Free carbon
As-formed	68.3	30.3	1.5	2.7	95.7	1.6
Annealed at 1800 °C	70.5	29.3	<0.2	0.4	98	0

Nuclear magnetic resonance (NMR) experiments were performed at room temperature on a Bruker MSL300 spectrometer operating at 75 MHz for ^{13}C nuclei and at 59 MHz for ^{29}Si. The spectra were recorded using a MAS probe with the sample spinning at 10 kHz. A single pulse acquisition sequence $[\pi/2, acq]$ with phase cycling (CYCLOPS) [7] was used. $\pi/2$ is the rotation of the magnetization from its equilibrium state and acq is the acquisition period. Several acquisitions were needed to obtain a good signal/noise ratio. The delay between pulses was varied from 10 s to 90 min. This delay takes into account the spin-lattice relaxation time (T_1) and generally 90% of the magnetization returns to the equilibrium position after $\tau_p \sim 5T_1$. Then, by varying τ_p, we were able to perform a selective detection of nuclei with different T_1. This is of particular importance when different local orders and a heterogeneity coexist in the material.

Table 2. Specific surface ($m^2\ g^{-1}$) and mean particle diameter (nm) at different annealing stages as determined by Brunauer–Emmet–Teller experiments.

Annealing temperature (°C)	Specific surface ($m^2\ g^{-1}$)	Equivalent diameter (nm)
As-formed	70	27
1200	72	26
1300	64	30
1400	35	54
1500	5	390
1550	6	310
1600	3	625
1650	2	937
1700	1	1560
1800	1	1600

EPR experiments were carried out on a Bruker ER-200D spectrometer equipped with different frequency bands (S (4 GHz), X (10 GHz) and K (24 GHz)). Additional measurements were also performed at Q (34 GHz) and W bands (95 GHz) where EPR spectra are highly sensitive to the anisotropy of the interactions. In all the investigated samples, the high unpaired spin concentration (10^{20}–10^{18} spin g^{-1}) limits the used microwave power to 2 mW and the modulation field to 0.5 G. The absolute concentration (N_s) of paramagnetic species is determined by a comparison with $CuSO_4$, $5H_2O$ single crystal ($\approx 3 \times 10^{21}$ spin g^{-1}).

In the following, different SiC212 samples are notated by their annealing temperature, e.g. S1200 for the sample annealed at 1200 °C, S1650 for the sample annealed at 1650 °C, etc.

3. Structural investigations by NMR

^{29}Si MAS NMR spectra of the S1200 and S1700 samples were recorded using a pulse period of $\tau_p = 90$ min (figure 1). In the S1200 sample, the spectrum shows superposition of Lorentzian lines at positions -15.2, -20 and -25 ppm and -16 ppm with respect to the tetramethyl silane used as a reference. The first three chemical shifts are those of ^{29}Si nuclei in the hexagonal α-SiC structure [8, 9]. The average line width of less than 1.5 ppm implies crystalline order of the α-SiC polytype in the S1200 sample. The fourth sharp line (-16 ppm) is attributed to the cubic β-SiC structure [10]. The pulse delay for spectra acquisition was set large with respect to the expected nuclear spin-lattice relaxation times ($T_1 \approx 35$ min) in these structures [10]. The integrated line intensities then give the weight of the coexisting structures. The proportion of cubic structure in the network is found to be close to 27% and the α-SiC polytype is present in a proportion of at least about 40%. The coexistence of disordered or amorphous SiC gives rise to a supplementary broad band (width 6 ppm) centred around -9 ppm, having a contribution to the spectrum of about 12%. Annealing at 1400 °C favours the development of β-SiC structure; its relative proportion increases to 60% in contrast to the α-SiC structure whose proportion is reduced to about 30%. Amorphous or disordered SiC regions remain. They show a relative contribution to the NMR spectrum of 10%.

In addition to the above SiC polytypes identified by ^{29}Si MAS NMR, ^{13}C MAS NMR spectra show the existence of polyaromatic carbon or graphitic clusters giving rise to a broad band (width 38 ppm) centred at 120 ppm (figure 1). Carbon excess is generally introduced during the fabrication process with a ratio [C]/[Si] $\approx$ 1.04 in the SiC212 sample. Carbon agglomerates are then formed and give rise to the broad band associated with disordered sp^2 carbon.

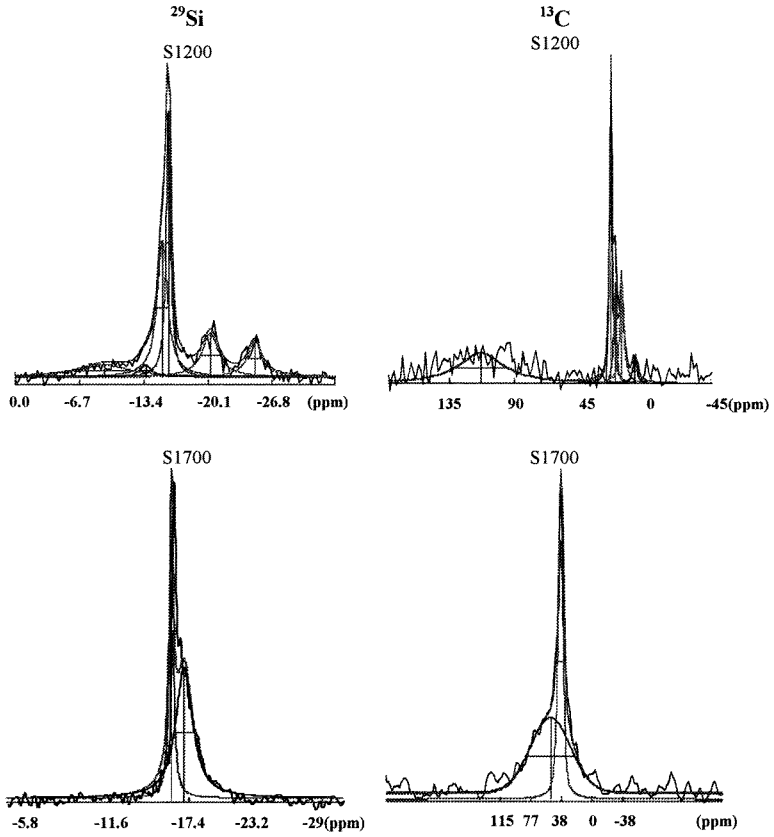

Figure 1. Experimental NMR spectra in samples S1200 and S1700 recorded using ^{29}Si and ^{13}C MAS with a pulse period $\tau_P = 90$ min. Deconvolution of the ^{29}Si spectra, summarized in table 3, yields the coexistence in S1200 of α-SiC, β-SiC and amorphous SiC. In the S1700 sample, a sharp line associated with β-SiC is superimposed on a shoulder the origin of which is discussed in the text. Deconvolution of the ^{13}C spectra gives the parameters summarized in table 4.

Table 3. Deconvolution results of the ^{29}Si MAS NMR spectra by Lorentzian lines in SiC nanomaterials annealed at 1200 °C and 1700 °C.

Sample	Line position (ppm)	Line width (ppm)	Integrated intensity ratio (%)	Assignment
S1200	−9.2	6.3	11.7	amorphous SiC
	−15.9	0.6	26.6	β-SiC
	−20.3	2.1	15.9	α-SiC
	−25.0	1.8	11.0	α-SiC
	−15.3	1.3	31.6	α-SiC
S1700	−15.9	0.4	33.5	β-SiC
	−17.0	1.7	66.5	structural defects or effects of paramagnetic centres in β-SiC

In all the SiC batches studied, annealing at $T \geqslant 1500$ °C was found to induce structural modifications $\alpha \rightarrow \beta$-SiC and removal of the sp^2 carbon contribution. Furthermore, the sharp NMR line associated with the cubic β-SiC structure is superimposed on a broad shoulder

Table 4. Deconvolution results of the ^{13}C MAS NMR spectra by Lorentzian lines in SiC nanomaterials annealed at 1200 °C and 1700 °C.

Sample	Line position (ppm)	Line width (ppm)	Integrated intensity ratio (%)	Assignment
S1200	114	38	45	free carbon
	23.5	1.95	27.7	α, β-SiC
	20.6	1.98	8.7	α-SiC
	15.8	3.4	15	α-SiC
S1700	22	3.7	36.6	β-SiC
	27.8	27.2	63.4	structural defects or effects of paramagnetic centres in β-SiC

(figure 1) which exhibits an enhanced intensity after reducing the pulse period (τ_p). These features can be understood as due to the coexistence of ^{29}Si and ^{13}C nuclei with large relaxation times (T_1) involved in well ordered crystalline regions and nuclei with short T_1 corresponding to disorder or electric conduction in these materials.

4. EPR investigations

Typical EPR spectra in S, X, K and W bands recorded at room temperature are shown in figure 2. A structured resonance line is common to all the EPR spectra with details depending on the used EPR frequency. Due to the critical annealing temperature $T_a = 1500$ °C, the S1200 and S1650 samples, representative of the SiC212 batch, were investigated at different EPR frequency bands and in the temperature range 4 K–300 K. By using two independent and complementary numerical procedures, we were able to analyse coherently the EPR spectra in these SiC nanopowders. The first procedure determined the overall spin susceptibility χ_s via numerical integration of the whole EPR spectrum. The second approach was based on deconvolution of the EPR spectrum in terms of coexisting paramagnetic centres, the spectroscopic data ($\tilde{g}$ and $\tilde{A}$ tensors) and relative concentrations of which were determined.

4.1. Spin susceptibility

The overall spin susceptibility χ_s, proportional to the integrated intensity of the whole EPR spectrum, was deduced by numerical integration of the EPR signal in both S1200 and S1650 samples. The product $\chi_s T$, depicted in figure 3, exhibits different behaviour for cross-over temperatures around 150 K and 30 K.

From 300 K to 150 K, the product $\chi_s T$ is temperature dependent and indicates that some of the paramagnetic centres are delocalized. The weakly positive slope obtained in the S1200 sample corresponds to Pauli-like paramagnetism thermally induced above 150 K. This is no longer valid in the S1650 sample where the negative slope of $\chi_s T$ is not yet understood. Spinless species or delocalized unpaired spins with short relaxation times with respect to the characteristic time scale of EPR ($\propto 1/\nu_{EPR}$) can be noted but further analysis is required for an understanding of the observed behaviour in the S1650 sample.

From 150 K to 4 K, the product $\chi_s T$, constant down to approximately 75 K, exhibits an increase and a sharp peak around 30 K in the S1650 sample (figure 3). Similar but less marked effects are also noticed in the S1200 sample. In the meantime, for both samples, the whole EPR spectrum line width ($\Delta H_{pp}(T)$) is enhanced below 30 K such that $\Delta H_{pp}(4\text{ K})/\Delta H_{pp}(30\text{ K}) \approx 5$. All these features are consistent with paramagnetic centres

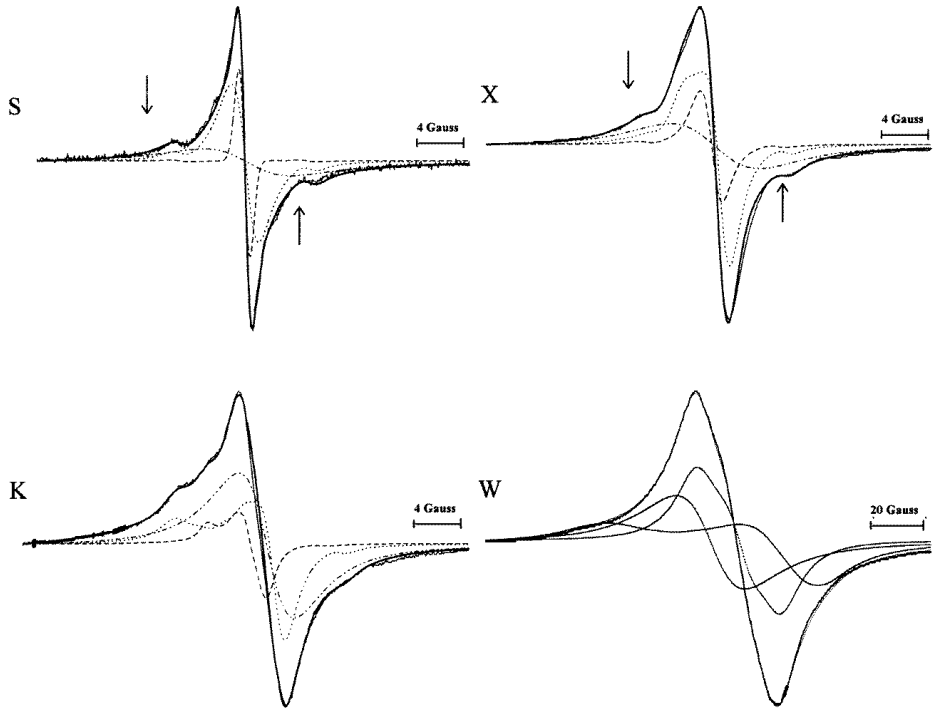

Figure 2. Room-temperature EPR spectra in the S1200 and S1650 samples recorded with different EPR frequency bands (S, $\nu = 4$ GHz; X, $\nu = 9.5$ GHz; K, $\nu = 24$ GHz; and W, $\nu = 95$ GHz). Simulations of these spectra are also shown.

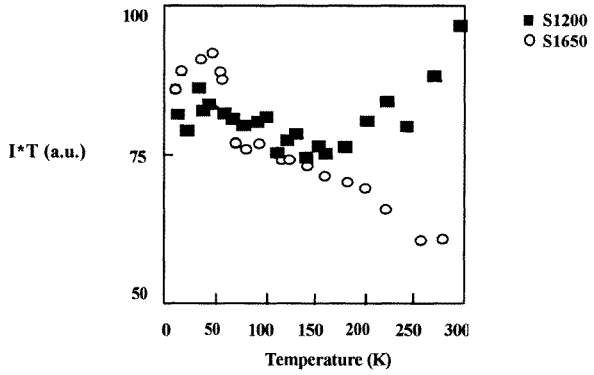

Figure 3. Representation of the product $\chi_s T$ (χ_s is the overall spin susceptibility) versus temperature for the S1200 and S1650 samples. Different behaviour is shown with cross-over temperatures around 150 K and 30 K. The electric conductivity versus S1650 sample temperature is also shown. The used EPR frequency was $\nu = 9.5$ GHz (X band).

being localized below 150 K and with strong correlation between unpaired spins realized in the S1650 sample around 30 K.

Table 5. EPR data of the DI, DII and DIII paramagnetic centres in SiC nanopowders, including the $\tilde{g}$ and $\tilde{A}$ tensors.

DI $g_x^I = 2.0044(2)$; $g_y^I = g_z^I = 2.0024(1)$	$A_x^I = A_y^I = A_z^I = 11 \times 10^{-4}$ cm^{-1}
DII $g_x^{II} = 2.0036(1)$; $g_y^{II} = 2.0026(1)$; $g_z^{II} = 2.0030(1)$	$A_x^{II} = A_y^{II} = A_z^{II} = 11 \times 10^{-4}$ cm^{-1}
DIII $g_x^{III} = g_y^{III} = g_z^{III} = 2.0031(2)$	No-hyperfine coupling

4.2. Numerical deconvolution of the EPR spectra

According to the procedure described previously for SiC and SiOC nanomaterials [11], the paramagnetic centres are $S = 1/2$ defects interacting with N equivalent neighbouring nuclei of ^{29}Si or ^{13}C (nuclear spin $I = 1/2$) and with an applied magnetic field $\vec{H}_{st}$. Each paramagnetic centre is described by the following spin Hamiltonian:

$$H_{Spin} = \beta \vec{H}_{st} \tilde{g} \vec{S} + \vec{S} \tilde{A} \vec{I}.$$

The adjustable parameters are the components of the $\tilde{g}$ and $\tilde{A}$ tensors, the individual resonance line width and the relative contribution to the EPR spectrum when coexisting paramagnetic centres are involved. On the other hand, due to the natural abundance (na) of ^{29}Si and ^{13}C, the EPR spectrum of a given paramagnetic defect is a superposition of two contributions. One is related to a spectrum with a hyperfine interaction, weighted by Nna, superimposed on a spectrum without hyperfine interactions weighted by $100 - Nna$.

By using this approach we were able to adjust the X band EPR spectra in all the samples annealed between 1200 °C and 1800 °C. Three paramagnetic defects (DI, DII and DIII) are involved; their parameters are summarized in table 5. Their contributions to the EPR spectrum are reported in figure 4 versus annealing temperature and in figure 5 versus the S1200 and S1650 sample temperature. The S, K and W band EPR spectra of the S1200 and S1650 samples are also consistent with the above deconvolution. This is of a particular importance for the relevance of the spectroscopic data and numerical analysis of the EPR spectra. Lack of precision in the deconvolution process occurs only below 30 K where the EPR spectra exhibit broadening and less highly resolved detail.

5. Discussion

The paramagnetic species DI and DII are characterized by anisotropic $\tilde{g}$ tensors, hyperfine structures and sharp individual resonance lines ($\Delta H_{pp} \leqslant 2$ G). These features can be understood by consideration of the paramagnetic centres localized in well organized environments, i.e. in the coexisting hexagonal and cubic sites of the α-β-SiC polytypes. The nature of the paramagnetic centres can be assessed from the shift of the $\tilde{g}$ tensor components with respect to the free electron factor ($g_e = 2.0023$) and from the magnitude of the hyperfine coupling constants. Qualitatively, the shifts ($\Delta g_\parallel = \Delta g_x = g_x - g_e = 0.0021$ and $\Delta g_\perp = \Delta g_y = \Delta g_z = 0$) for DI species are not consistent with dangling bonds (DBs) located on one silicon or carbon atom. Indeed, taking the DB direction as the $\tilde{g}$ tensor X-axis, axial symmetry will imply opposite shifts ($\Delta g_x = 0$ and Δg_y; $\Delta g_z \neq 0$) with respect to the obtained values for DI centres. This is supported by a quantitative analysis of the hyperfine interaction between the unpaired spins and the surrounding ^{13}C or ^{29}Si nuclei. Indeed, for DI or DII centres, the hyperfine lines contribute to the EPR spectrum by a ratio $Nna = 10\%$. This implies a coupling between an unpaired spin with nine equivalent carbon or with two equivalent silicon atoms. Let us first examine the case where the hyperfine coupling implies involvement of a silicon atom. The wave function of the molecular complex with an unpaired spin can be

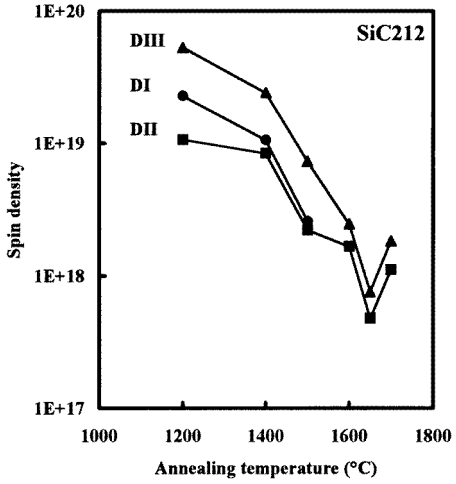

Figure 4. Concentration of the different paramagnetic centres, at room temperature, versus annealing temperature of the SiC nanomaterials.

expressed as a linear combination of the silicon wave functions and the surroundings atoms as follows:

$$\Psi_{DI,DII} = \alpha\Psi_{3s}(Si) + \beta\Psi_{3p}(Si) + \gamma\Psi_{env.}.$$

$\Psi_{3s}(Si)$ and $\Psi_{3p}(Si)$ are related to Si atoms and $\Psi_{env.}$ refers to the contribution to a defect wave function from other surrounding atoms.

The isotropic A_{iso} (Fermi contact) and the anisotropic A_{aniso} (dipolar contribution) hyperfine constants for a free atom are given by:

$$A_{iso} = \frac{2}{3}\mu_0 g_e g_{Si}\mu_B\mu_n|\Psi_{3s}(0)|^2$$

$$A_{aniso} = \frac{2}{5}\frac{1}{4\pi}\mu_0 g_e g_{Si}\mu_B\mu_n\left\langle\frac{1}{r^3}\right\rangle_{|\Psi_{3p}\rangle}$$

where $\mu_0 = 4\pi \times 10^{-7}$ H m^{-1}, g_e is the free electron Landé factor (2.0023), $g_{Si} = -1.1106$ is the nuclei Landé factor, μ_B and μ_n are respectively the Bohr and the nuclear magneton and (r, θ, φ) represents the unpaired electron coordinates with respect to a frame centred on the nucleus.

The Hartree–Fock wave functions of a free silicon atom [12] are used to estimate the following quantities:

$$|\Psi_{3s}(0)|^2 = 37 \times 10^{24}\ \text{cm}^{-3}$$

$$\left\langle\Psi_{3p}\left|\frac{1}{r^3}\right|\Psi_{3p}\right\rangle = 24 \times 10^{24}\ \text{cm}^{-3}.$$

Then, the theoretical values are $A_{iso} = 1573 \times 10^{-4}$ cm^{-1} and $A_{aniso} = 32 \times 10^{-4}$ cm^{-1}. Experimentally, these parameters are determined from the $A_\parallel$ and $A_\perp$ values of the axially symmetric hyperfine tensor as follows:

$$A_{iso} = \tfrac{1}{3}(A_\parallel + 2A_\perp)$$

$$A_{aniso} = \tfrac{1}{3}(A_\parallel - A_\perp).$$

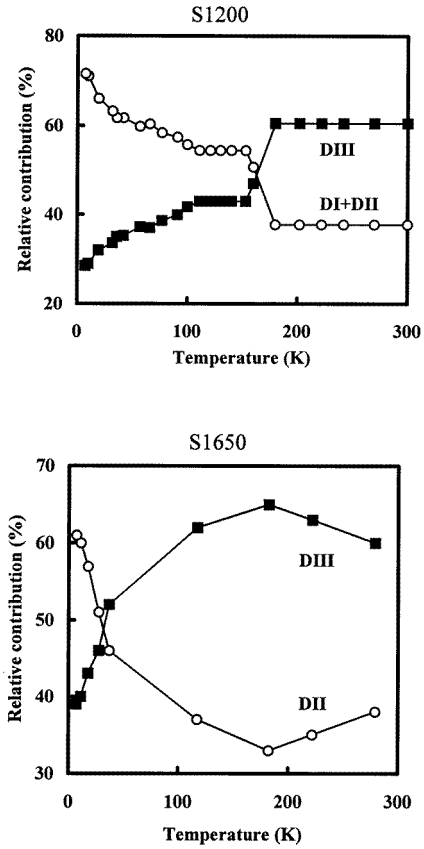

Figure 5. Relative contribution of the three paramagnetic defects to the EPR X band spectrum ($\nu = 9.5$ GHz) versus temperature of the S1200 and S1650 samples. A conversion process between paramagnetic centres is observed and requires thermal energies below 13 meV.

The experimental hyperfine tensor is isotropic at room temperature with the parameter $A_{iso}^{exp} = 11 \times 10^{-4}$ cm^{-1}. Then, the contribution from the silicon 3s orbital to the defect wave function is of the order of $|\alpha|^2 = A_{iso}^{exp}/A_{iso} \approx 0.6\%$. The same treatment is applied in the case of hyperfine coupling with ^{13}C atoms. According to Luchsinger *et al* [13], the theoretical hyperfine constants for free ions are $A_{iso}^{free}(^{13}\mathrm{C}) \approx 1260 \times 10^{-4}$ cm^{-1}, $A_{iso}^{free}(^{13}\mathrm{C}) \approx 33 \times 10^{-4}$ cm^{-1}. The unpaired electron probability in the s orbital of carbon is

$$|\alpha|^2(^{13}\mathrm{C}) \approx 0.6\%$$

so no more than 1% of the spin density is accounted for by the localization of the unpaired spin on a silicon or a carbon nucleus. We may conclude that DI and DII paramagnetic centres are not compatible with DBs localized on given atoms. These centres are more consistent with unpaired spins delocalized inside the hexagonal and cubic SiC sites.

In contrast to the above paramagnetic centres, DIII species exhibit quite different features. They give rise to a broad Lorentzian line which brings, at room temperature, a relative contribution of about 60% to the EPR spectrum. Disordered SiC regions or carbon agglomerates can give rise to such a background absorption line. However, by varying ν_{EPR}, we have not observed any line broadening (ΔH_{pp}) connected with a spread of the $\tilde{g}_{III}$ components

which may be caused by structural disorder around DIII defects. In samples S1200 and S1650, the line widths $\Delta H_{pp}^{X}(\mathrm{S1200}) = 8$ G and $\Delta H_{pp}^{X}(\mathrm{S1650}) = 5$ G in the X band change to $\Delta H_{pp}^{W}(\mathrm{S1200}) = 13$ G and $\Delta H_{pp}^{W}(\mathrm{S1650}) = 6$ G in the W band. If disorder induces a spread of g values, the ratio between the line widths will be close to

$$\frac{\Delta H_{pp}^{W}}{\Delta H_{pp}^{X}} \approx \frac{\nu_{EPR}^{W}}{\nu_{EPR}^{X}} \approx 10.$$

This criterion rules out the location of DIII defects in disordered material regions. Furthermore, the relative contributions of the different paramagnetic centres (figure 5) show the same behaviour around 150 K in both S1200 and S1650 samples. This is in agreement with the overall spin susceptibility determined above via using an independent approach. A conversion between paramagnetic centres explains the anti-coincidence of the contribution from the localized DI, DII centres and that from DIII species. Such a conversion process needs thermal energies below 13 meV and will induce delocalized paramagnetic centres of DIII type.

Finally, let us discuss the correlation between the delocalized paramagnetic centres and the electric properties originally evidenced in these materials in the EPR results. Indeed, when inserting the S1650 sample in the EPR resonant cavity, damping of the cavity is induced in a similar manner as in the case of metallic materials. This phenomenon is dramatically enhanced by suitable design of the resonant cavity in order to locate the sample in the region where the microwave electric field is maximal. However, in the case of SiC nanomaterials, neither the whole EPR spectrum linewidth nor the individual resonance linewidths follow the linear decrease expected in metallic-like materials (Korringa effect). So, the severe damping of the resonant cavity by the S1650 sample can be explained by dielectric losses consistent with electric conductivity. We therefore performed quantitative electric measurements which will be reported in detail elsewhere. Only a weak and thermally activated conductivity ($\sigma_{dc} \sim 10^{-6}$ S cm^{-1} at 400 K) was found in sample S1400 sample. By contrast, a significant and irreversible electric conductivity ($\sigma_{dc}(T) = 0.05$ S cm^{-1} at 300 K), determined by the four-probe method, was found in sample S1650 (figure 3). The variation law $\sigma(T) = \sigma_0 \, \mathrm{e}^{-E_g/kT}$ indicates a thermally activated conductivity with variable energy—$E_g \approx 2$ meV below approximately 185 K and $E_g \approx 35$ meV above. Electronic transport measurements (Hall effect) yield n-type electronic conduction with a charge carrier density close to 10^{19} cm^{-3}.

DIII centres can eventually participate in conduction phenomena in these materials. Indeed, their concentration and thermal activation energies (obtained by EPR) are of the same order of magnitude as those determined by conduction and electronic transport measurements. n-type charge carriers with a density of about 10^{19} cm^{-3} in sample S1650 correlate to a DIII concentration of 10^{18} spin g^{-1} in S1650 (figure 4). On the other hand, the conductivity is thermally activated for an energy $E_g \approx 2$ meV and this value jumps to 35 meV above 185 K. These energy gaps are correlated with the thermal energies which induce delocalized DIII unpaired spins from localized DII species.

However, even if delocalized DIII species are present with a relative contribution at room temperature close to 60%, the conductivity of samples annealed below $T_a = 1500\,^{\circ}$C seems to be limited by interface barriers. All the investigated SiC batches contain a carbon excess such that $1.04 \leqslant ([\mathrm{C}]/[\mathrm{Si}])_{at} \leqslant 1.10$. We have shown that the carbon excess is predominantly located at the outermost particle surface [14] and acts as a barrier for the conduction channels. By annealing above $T_a = 1500\,^{\circ}$C, elimination of the carbon excess and increase of the mean particle diameter favour the development of macroscopic conduction. It is worth pointing out here that the grain size is not crucial to the conduction phenomena. The three batches (SiC163, SiC177 and SiC212) showed similar electric properties when annealed at 1500 °C but their mean particle diameter changed to differing degrees, as reported above (section 2). It seems

that, in these materials, a more crucial role is played by the carbon excess in these materials and by the ratio of the cubic crystalline sites of SiC polytypes where the unpaired spins have shallower levels that are easily activated by low thermal energies.

6. Conclusion

The structural modifications in SiC nanomaterials as a result of annealing were monitored by ^{29}Si and ^{13}C MAS NMR. The critical annealing temperature was found to be close to 1500 °C. At this temperature the structure changes from $\alpha \rightarrow \beta$-SiC and this is accompanied by a substantial and irreversible electric conductivity. EPR investigations using different frequency bands (4–95 GHz), low- and high-temperature measurements and consistent numerical EPR spectrum analyses were carried out. We have shown that the paramagnetic centres in these SiC nanomaterials consist of localized unpaired spins in the crystalline sites of the SiC polytypes superimposed on sites of delocalized spins. The latter have thermal activation energies and concentrations related to the corresponding parameters determined by electric measurements.

Acknowledgment

We are indebted to Professor S Rolland (INSA-Rennes) for electric measurements on the S1650 sample.

References

[1] Niihara K 1991 *J. Ceram. Soc. Japan* **99** 974
[2] Baronnet J M 1992 *High Temp. Chem. Process* **1** 577
[3] Haggerty J S, Suyama Y, Marra R A and Bowen H K 1985 *Am. Ceram. Soc. Bull.* **60** 1356
[4] Cauchetier M, Croix O and Luce M 1988 *Adv. Ceram. Mater.* **3** 548
[5] Cauchetier M, Croix O, Luce M, Baraton M I, Merle T and Quintard P 1991 *J. Europ. Ceram. Soc.* **8** 215
[6] Charpentier S 1998 *PhD Thesis* Université du Maine, France
[7] Homans S W 1992 *A Dictionary of Concepts in NMR* (Oxford: Clarendon)
[8] Hartman J S, Richardson M F, Sheriff B L and Winsborrow B G 1987 *J. Am. Chem. Soc.* **109** 6059
[9] Carduner K R, Shinozaki S S, Rokosz M J, Peters C R and Whalen T J 1990 *J. Am. Ceram. Soc.* **73** 2281
[10] Apperley D C, Harris R K, Marshall G L and Thompson D P 1991 *J. Am. Ceram. Soc.* **74** 777
[11] Charpentier S, Kassiba A, Fusil S, Cauchetier M, Armand X, Fayet J C and Emery J 1997 *Appl. Magn. Reson.* **12** 255
[12] 1974 *Atomic Data and Nuclear Data Tables* vol 14, nos 3–4 (Clementi and Roetti)
[13] Luchsinger R H, Zhou Yu and Meier P F 1997 *Phys. Rev.* B **55** 6927
[14] Charpentier S, Kassiba A, Bulou A and Cauchetier M to be published